1989

Bending Shear: The Rate-Controlling Mechanism for Calving Ice Walls

Terence J. Hughes
University of Maine - Main, terry.hughes@maine.edu

Masayuki Nakagawa

Journal of Glaciology, Vol. 35, No. 120, 1989

BENDING SHEAR: THE RATE-CONTROLLING MECHANISM FOR CALVING ICE WALLS*

By TERENCE HUGHES

(Institute for Quaternary Studies and Department of Geological Sciences, University of Maine, Orono, Maine 04469, U.S.A.)

and MASAYUKI NAKAGAWA

(Kanazawa Women's Junior College, Kanazawa, Ishikawa 920-13, Japan)

ABSTRACT. Bending shear was observed to produce nearly vertical shear bands in a calving ice wall standing on dry land on Deception Island (lat. 63.0°S., long. 60.6°W.), and slabs calved straight downward when shear rupture occurred along these shear bands (Hughes, 1989). A formula for the calving rate was developed from the Deception Island data, and we have attempted to justify generalizing this formula to include ice walls standing along beaches or in water. These are environments in which a wave-washed groove develops along the base of the ice wall or along a water line above the base. The rate of wave erosion provides an alternative mechanism for controlling the calving rate in these environments. We have determined that the rate at which bending creep produces nearly vertical shear bands, along which shear rupture occurs, controls the calving rate in all environments. Shear rupture occurs at a calving shear stress of about 1 bar. Our results justify using the calving formula to compute the calving rate of ice walls in computer models of ice-sheet dynamics. This is especially important in simulating retreat of Northern Hemisphere ice sheets during the last deglaciation, when marine and lacustrine environments were common along retreating ice margins. These margins would have been ice walls standing along beaches or in water, because floating ice shelves are not expected in the ablation zone of retreating ice sheets.

INTRODUCTION

Slabs calve from ice walls along shear bands that rise vertically from the base of the ice wall and curve slightly toward the ice wall (Hughes, 1989). Shear strain in shear bands increases from zero at the base, which is a rigid boundary, to a maximum at the surface, which is a free boundary. In this respect, slip in shear bands is analogous to slip between pages of a book when the book is bent around its binding, where the binding is a rigid boundary. Based on this mechanism, a formula for the calving rate of slabs from an ice wall was derived in which calving rate u_c is:

$$u_c = u_s c/h\theta \cong u_s cR/h^2 \qquad (1)$$

where u_s is the horizontal surface velocity of ice at the top of the ice wall, c is the horizontal distance between the ice wall and transverse crevasses immediately behind the ice wall, h is the height of the ice wall, θ is the angle through which the ice wall bends to produce the curving shear bands, and $R \cong h/\theta$ is the radius of bending curvature of the shear bands (Hughes, 1989). For steady-state calving, $u_c = \bar{u} = ku_s$, where $\bar{u}$ is the mean forward velocity of the ice wall and k is a constant. Therefore, $c = kh\theta \cong kh^2/R$ in Equation (1).

By definition, ice walls are grounded in water whose depth ranges from zero to the depth needed to float ice having the height of the ice wall. Equation (1) was derived using data obtained from an ice wall standing on dry land. When an ice wall stands in the intertidal zone of a beach, a wave-cut groove exists along the base of the ice wall. This groove exists along the water line when the ice wall is grounded in water. In addition, inhomogeneous creep in the

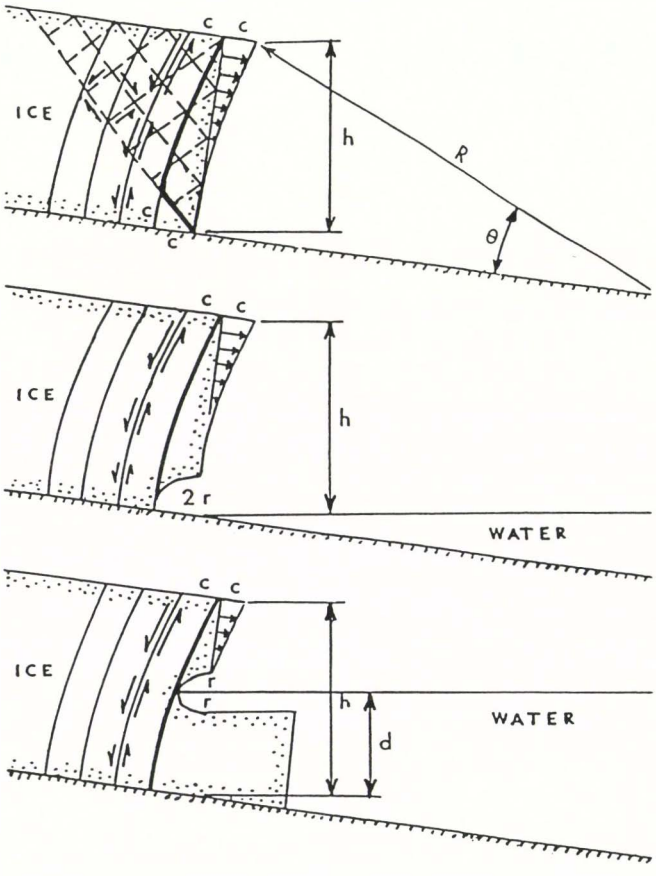

Fig. 1. The bending creep mechanism for shear rupture in calving ice walls. Ice walls are shown grounded on dry land (top), at the shoreline of a beach (middle), and in deep water (bottom). Straight dashed lines intersecting the ice wall at 45° are the slip lines of maximum shear stress for homogeneous creep, curving solid lines rising vertically from the bed are shear bands produced by bending creep. Heavy lines are calving surfaces for shear rupture.

* See *Annals of Glaciology*, Vol. 12, 1989, p. 204 for an extended abstract.

curving shear bands interacts with homogeneous creep between shear bands that is described by lines of maximum shear stress intersecting the ice wall at 45° angles and which constitute the slip-line field for plastic flow. These features are illustrated in Figure 1. They pose this question: is the rate of slab calving controlled by the rate at which bending creep produces curving shear bands, the rate at which shear rupture occurs along slip lines, or the rate at which grooves are produced by wave action? We wish to present our answer to that question.

ICE WALLS GROUNDED ON DRY LAND

The role of shear rupture along slip lines was deduced from observations of a calving ice wall grounded on dry land in an eruption crater on Deception Island (lat. 63.0°S., long. 60.6°W.), which lies off the Antarctic Peninsula. Four tunnels were dug at various heights up the ice wall, and a shallow groove was cut down the entire height of the ice wall (Hughes, 1989). These excavations revealed the bending shear mechanism shown schematically in Figure 2. The increase of bending shear with distance above the base of

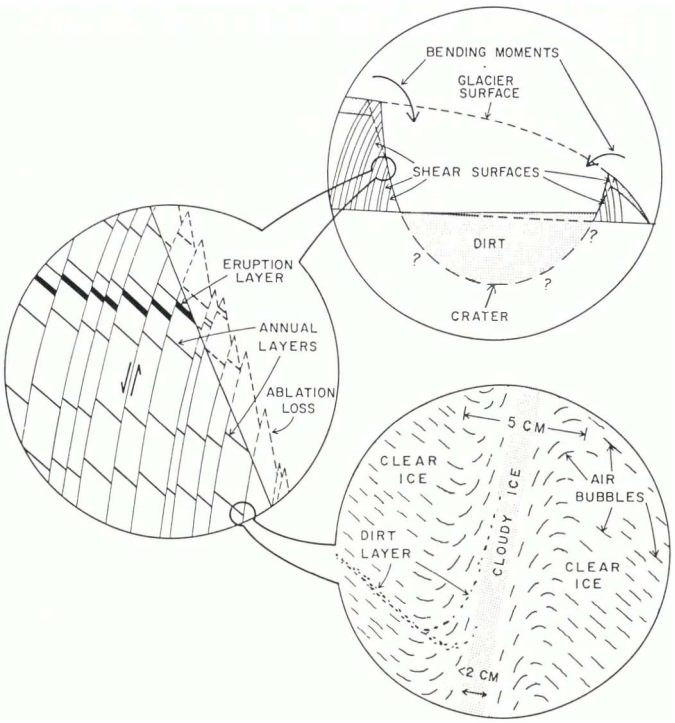

Fig. 2. A cartoon of the crater produced by the 12 August 1970 subglacial volcanic eruption on Deception Island. Details of the up-slope ice wall show offsets of ash and dust layers by shear bands produced by a bending movement (from Hughes, 1971).

the ice wall was revealed by increasing offsets of ash and dust layers intersected by the shear bands. We determined crystal fabrics from ice samples taken from these excavations.

An ice sample containing a shear band intersecting an ash layer is shown in Figure 3, and Figure 4 shows ice fabrics inside (Fig. 4a) and outside (Fig. 4b) of this shear band. Fabric (a) is the typical ice fabric in a shear band. It shows that optic axes (the crystallographic *c*-axes normal to easy-glide atomic planes of hexagonal symmetry) are strongly clustered near a pole at 90° to the plane of the shear band, and weakly clustered near a pole at 45° to this plane. Fabric (b) is the typical ice fabric between shear bands. It shows that optic axes are strongly clustered near a pole at 45° to the plane of the shear band and very weakly clustered near a pole at 0° to the plane of the shear band.

We interpret clustering of optic axes near the 90° pole as resulting from recrystallization within the shear band to produce an easy-glide ice fabric favoring inhomogeneous bending creep. We interpret clustering of optic axes near the 45° pole as resulting from homogeneous creep between

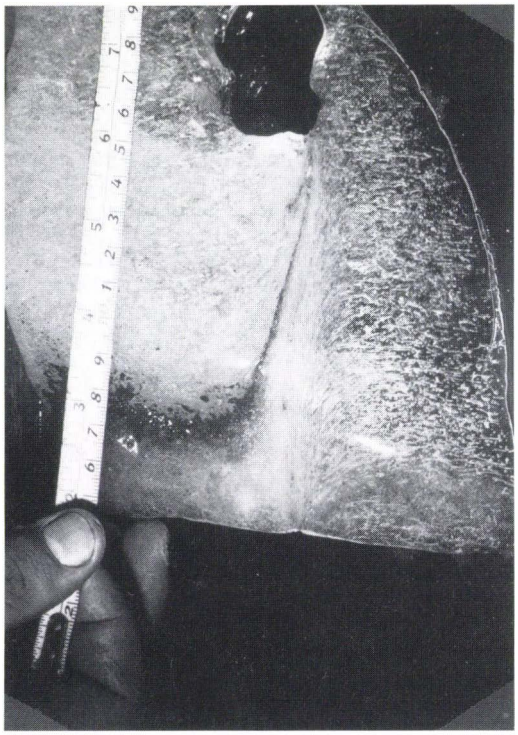

Fig. 3. A dirt layer and air bubbles drawn into a shear band in the calving ice wall on Deception Island.

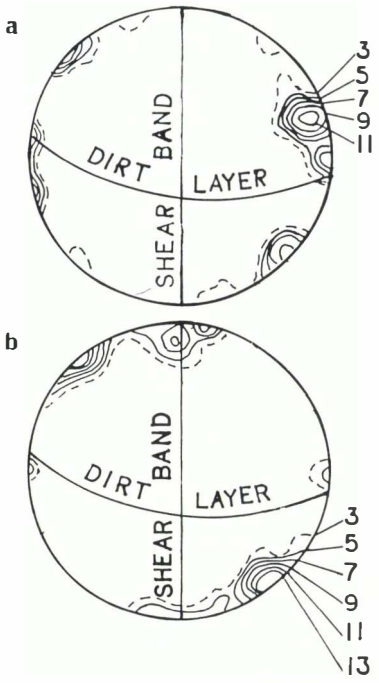

Fig. 4. Ice fabrics in a thin section of the ice sample in Figure 3. Fabric (a) is contoured from 61 poles inside the shear band. Fabric (b) is contoured from 80 poles outside the shear band. Numbers denote the per cent of c-axes per 1% of area in the Schmidt diagrams. The dirt layer in Figure 3 has the orientation shown.

shear bands to produce an easy-glide ice fabric favoring shear deformation along lines of maximum shear stress aligned at 45° to the ice wall (and, therefore, at nearly 45° to the shear bands), with this fabric predominating between shear bands and existing as a much weaker "ghost" fabric of unrecrystallized grains within shear bands. We interpret the very weak clustering of optic axes near the 0° pole observed between shear bands as resulting from basal traction, as this fabric becomes stronger in ice samples closer to the bed, and this pole is perpendicular to the bed, where basal traction tends to produce an easy-glide ice fabric having this pole orientation.

Actual observations of slab calving on the Deception Island ice wall show that the easy-glide fabric for inhomogeneous bending creep in shear bands is superimposed on an older easy-glide fabric for homogeneous creep in the direction of the slip-line field (Hughes, 1989). Slabs calve when easy glide in the shear bands drastically reduces coupling across shear bands and drastically enhances slip along shear bands. Since the shear bands are nearly vertical, up-glacier uncoupling means that virtually the entire weight of ice slabs between shear bands must be borne by ice at the base of these slabs. Shear rupture along a 45° plane near the base of the slab between the ice wall and the shear band will allow the slab to calve from the ice wall. Since the easy-glide ice fabric that exists in these 45° planes cannot lead to shear rupture until bending creep produces the easy-glide ice fabric in shear bands, bending creep is the rate-controlling process for slabs calved from ice walls grounded on dry land.

ICE WALLS GROUNDED ALONG A BEACH SHORELINE

Along the northern Antarctic Peninsula, most calving ice walls are grounded in the intertidal zone of beaches. Similar ice walls may have extended along the beach shorelines of pro-glacial lakes during retreat of North American and Eurasian ice sheets after the last glacial maximum about 14 000 years ago. Hence, slab calving from these ice walls is the dominant ablation mechanism for glaciers on the northern Antarctic Peninsula today and may have been an important ablation mechanism during the last deglaciation.

The dominant features of intertidal ice walls along Antarctic beaches are a continuous shoreline groove at the base of the ice wall and large cavities in re-entrant angles of the ice wall. Both features are eroded by wave action in the intertidal zone between high and low tides, supplemented by waves that accompany storms. The grooves and cavities are everywhere, except for sections of the ice wall that are fresh unweathered fracture surfaces. Personal observations of calving events along these ice walls during November and December of 1988 showed that slab calving was caused by nearly vertical shear rupture along transverse crevasses immediately behind the ice wall. Moreover, the fresh surface exposed after a slab calved had the slight concave curvature that was observed in the nearly vertical shear bands produced by bending creep in the ice wall we studied in detail on Deception Island.

If development of shear bands by bending creep along the intertidal ice walls of the Antarctic Peninsula precedes undercutting of the ice wall by wave action, then the tidal groove and re-entrant cavities should be the exception rather than the rule for these ice walls, because shear rupture would occur as soon as the groove and cavities had undercut ice back to the shear band closest to the ice wall. On the other hand, if bending creep produced shear bands more slowly than wave action produced the groove and cavities, these intertidal features would be almost ubiquitous, because they would develop long before shear rupture in the shear bands produced calving events. Since intertidal grooves and cavities exist at the base of intertidal ice walls along nearly all shorelines of the Antarctic Peninsula, except where slabs have recently calved, we conclude that bending creep producing shear bands along which shear rupture occurs is the rate-controlling mechanism for slab-calving.

ICE WALLS GROUNDED IN WATER

Calving ice walls standing in water exist along the margin of the Antarctic ice sheet everywhere except where the ice margin abuts mountains, forms an ice wall in the intertidal zone along beaches, or advances in water deep enough to float the ice and produce an ice shelf. Much of the Wilkes Land margin of the Antarctic ice sheet is an ice wall grounded in water. It is likely that retreating margins of the North American and Eurasian ice sheets during the last deglaciation often were ice walls grounded in sea-water along marine margins and in pro-glacial lakes along terrestrial margins. Slab calving is the dominant ablation mechanism where these ice walls exist in Antarctica today, and may have been an important ablation mechanism for retreating Northern Hemisphere ice sheets.

Wave-washed grooves form along the water line of ice walls grounded in water, and these grooves are enlarged into cavities in the re-entrant angles of the ice walls, where wave action is focused. Calving of ice slabs above the groove and cavities proceeds by the same mechanism that we observed for ice walls standing in the intertidal zone of beaches, where wave action produces a groove and cavities at the base of the ice wall. Under-water calving of ice beneath the wave-washed groove and cavities may also proceed by shear rupture along the shear bands produced by bending creep. The basic difference would be that shear rupture proceeds downward above the water line and upward below the water line.

In order for the calving rate to be the same above and below the water line, the downward gravity force and the upward buoyancy force that cause shear rupture above and below the wave-washed groove should produce identical calving stresses. Since the density of ice is about ten times the density difference between ice and water, slabs calved below the wave-washed groove must be about ten times larger than slabs calved above the groove if the upward and downward calving causes shear rupture at the same calving stress.

CALVING FORCES ON ICE WALLS

Nature abhors a vacuum, and air in front of an ice wall is a vacuum compared to ice in back of the ice wall, so a horizontal force exists that pulls the ice wall forward and opens transverse crevasses behind the ice wall. Shear rupture proceeds downward from these crevasses along shear bands produced by bending creep (Hughes, 1989). For orthogonal axes with x horizontal and perpendicular to the ice wall, y horizontal and parallel to the ice wall, and z vertical, the horizontal pulling force F_x calving a slab of width w from an ice wall of height h standing in water of depth d is:

$$F_x = \tfrac{1}{2}\rho_I g w h^2 - \tfrac{1}{2}\rho_W g w d^2 \qquad (2)$$

where ρ_I and ρ_W are ice and water densities and g is gravity acceleration. Pulling force F_x opens transverse crevasses behind the ice wall and induces a bending moment $M_y(z)$ at the base of the ice wall that produces the shear bands extending upward from the base of the ice wall to the tips of surface crevasses, and along which shear rupture occurs. From Hughes (1989):

$$M_y(z) = \frac{1}{6}\rho_I g w(h - z)^3 - \frac{1}{6}\rho_W g w(d - z)^3 \qquad (3)$$

where $z = 0$ and $z = h$ at the bottom and top of the ice wall, respectively. Notice that the bending moment decreases as water gets deeper, and vanishes at depth $d = (\rho_I/\rho_W)^{1/3}h$, which is greater than depth $d = (\rho_I/\rho_W)h$ at which the ice wall floats and thereby creates an ice shelf. Hence, a bending moment exists so shear bands can form even after the ice floats.

For an ice wall grounded on dry land, a slab having height h, width w, and thickness c calves when a vertical gravity force F_z causes shear rupture across the shear bands produced by bending creep. The calving slab then slides across the plane in the slip-line field that intersects both the shear band and the ice wall at a 45° angle. Hence, shear rupture occurs only along distance $h - c$ of the shear band and:

$$F_z = \rho_I g(h - c)wc\,. \qquad (4)$$

For an ice wall grounded in the intertidal zone of a beach, the basal groove and cavities eliminate shear rupture on the 45° planes and the calving force when the groove has radius r is:

$$F_z = \rho_I g(h - 2r)wc\,. \qquad (5)$$

For an ice wall grounded in water of depth d, the calving

force above the wave-washed groove and cavities is:

$$F_z = \rho_I g(h - d - r)wc \qquad (6)$$

and the calving force below the wave-washed groove and cavities is:

$$F_z = (\rho_I - \rho_w)g(d - r)wC \qquad (7)$$

where C is the calving distance behind the submerged part of the ice wall.

CALVING STRESSES ON ICE WALLS

The calving stress on an ice wall would be calving force F_c divided by the area across which shear rupture occurs. For an ice wall grounded on land, this would be area $w(h - c)$ of the shear band produced by bending creep and area $(2)^{\frac{1}{2}}cw$ of the plane that lies in the slip-line field and intersects both the ice wall and the basal part of the shear band at a 45° angle. Since the rate of slab calving is controlled by shear rupture across the shear band, which has the larger area and therefore the lower stress for shear rupture, the calving stress is:

$$\tau_c = \frac{\rho_I g(h - c)wc}{(h - c)w} = \rho_I gc\,. \qquad (8)$$

For an ice wall grounded in the wave-washed zone of a beach, shear rupture occurs only across shear bands produced by bending creep so that:

$$\tau_c = \frac{\rho_I g(h - 2r)wc}{(h - 2r)w} = \rho_I gc\,. \qquad (9)$$

For an ice wall grounded in water, shear rupture above the water line occurs for:

$$\tau_c = \frac{\rho_I g(h - d - r)wc}{(h - d - r)w} = \rho_I gc \qquad (10)$$

and shear rupture below the water line occurs for:

$$\tau_c = \frac{(\rho_I - \rho_w)g(d - r)wC}{(d - r)w} = -\rho_I gc \qquad (11)$$

where Equations (10) and (11) must be equal for the calving rate to be the same above and below the wave-washed groove and cavities, so that:

$$C = \frac{c\rho_I}{\rho_w - \rho_I}\,. \qquad (12)$$

Since c = 10 m is a typical slab thickness between the ice wall and the first transverse crevasse, Equations (8) through (11) give $|\tau_0|$ = 1 bar = 100 kPa for the absolute value of the calving stress. Hence, it appears that a bending shear stress of about 1 bar is required to generate the easy-glide ice fabrics in shear bands that facilitate shear rupture.

Our only evidence that Equation (12) holds was our observation of a submarine calving event on San Rafael Glacier in the Chilean fjords on 21 November 1988. The submarine block that rose to the surface was about ten times larger than slabs calved above a wave-washed groove 3 m deep. The ice wall extended 100 and 50 m above and below sea-level near the fjord walls, and 130 and 120 m above and below sea-level near the center of the fjord, where the calving event occurred. Setting ρ_I = 920 kg/m^3 for ice and ρ_w = 1020 kg/m^3 for sea-water gives $C = 9.2c$ in Equation (12). Other evidence that blocks calved below sea-level are much larger than slabs calved above sea-level for ice walls grounded in water is figure 28 from Post and LaChapelle (1971), a photograph showing these blocks and slabs floating in front of the South Sawyer Glacier calving ice wall in south-east Alaska.

We conducted laboratory creep experiments in which simple shear predominated, and we determined the shear stress needed to create an easy-glide ice fabric in a shear band of the same thickness as those produced by bending shear on the Deception Island calving ice wall. A polycrystalline ice specimen having a random orientation of crystal grains was produced by packing snow into a mold 75 mm by 75 mm by 220 mm, saturating the snow with cold water, and freezing the mixture. This produced grains of about 1 mm in diameter. The sample was then removed from the mold and each end was frozen into twin box grips, 75 mm long, 75 mm wide, and 100 mm deep, of the creep machine shown schematically in Figure 5. Weights hung on the chain from the large-diameter wheel transmitted a constant shear stress to the 75 mm by 75 mm cross-section of ice exposed between the two box grips, by means of a chain from the small-diameter wheel.

As seen in Figure 5, the box grips moved in nearly frictionless ball-bearing housings, with vertical motion of

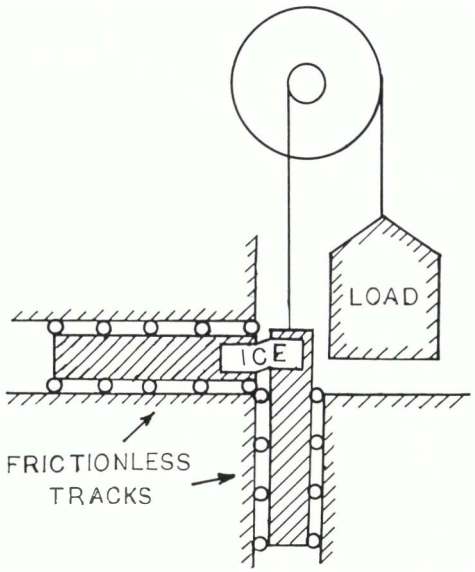

Fig. 5. A schematic diagram showing the configuration of specimen grips and the applied load for simple shear-creep experiments. The creep machine is designed to conduct creep experiments in simple shear, uniaxial tension, uniaxial compression, and torsion, with constant stress in the uniaxial tests maintained using a variable lever-arm (Garofalo and others, 1962).

one box grip allowing simple shear in the exposed specimen and horizontal motion of the other box grip suppressing uniaxial tension in the exposed specimen. Taking rectilinear axes with x horizontal and normal to the plane of shear, y horizontal, and z vertical and both parallel to the plane of shear, as shown in Figure 6, the exposed volume of the ice specimen was $V = L_x L_y L_z$, where L_x could be varied, but $L_y = L_z$ = 75 mm is constant. The plane of shear initially had about 75 grains along L_z, making the production of an easy-glide ice fabric independent of the initial grain-size. When a load was applied, one box grip underwent vertical translation u_z and the other box grip underwent horizontal translation u_x. Vertical motion introduces shear stress τ_{zx} in volume V and causes shear strain ε_{zx}, where $2\varepsilon_{zx} = \tan\gamma = u_z/L_x$. Horizontal motion suppresses a tensile stress that would otherwise stretch volume V by an amount $(\sec\gamma - 1)L_x$. The only stresses are shear stress τ_{zx} and bending stress σ_{xx}, where volume V is bent near the box grips because the box grips do not rotate during translation u_z (Dehlinger, 1950; Read, 1950).

The distribution of σ_{xx} and τ_{zx} along L_z is provided by beam theory. For elastic deformation σ_{xx} varies linearly from $\sigma_{xx} = \sigma_m$ for maximum tension (convex bending) or compression (concave bending) at $z = \pm L_z/2$, to $\sigma_{xx} = 0$ at $z = 0$. For plastic deformation, $\sigma_{xx} = \sigma_m$ along L_z, but changes abruptly from tension to compression at $z = 0$. For elastic deformation, τ_{zx} varies parabolically from $\tau_{zx} = 0$ at $z = \pm L_z/2$ to $\tau_{zx} = \tau_m$ for maximum shear at $z = 0$. For plastic deformation, $\tau_{zx} = \tau_m$ along most of L_z,

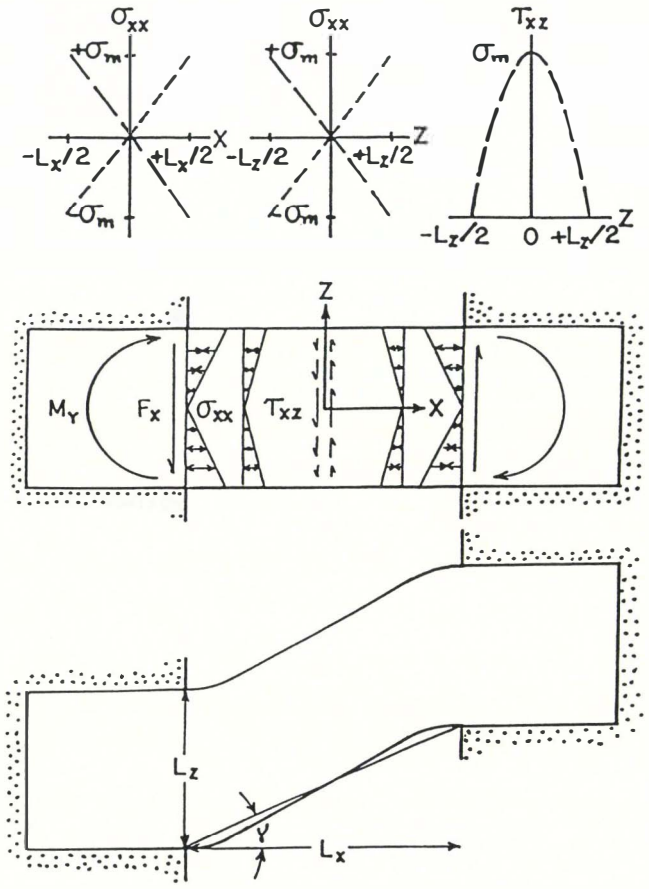

Fig. 6. Stresses and deformation of an ice specimen mounted in the simple shear-creep configuration shown in Figure 5. Top: the distribution of elastic shear stress τ_{zx} and bending stress σ bending moment M_y at the onset of creep deformation. Bottom: the distribution of viscoplastic shear and bending produced by strain γ at the conclusion of creep deformation. Bending is suppressed when $L_x << L_z$.

except at $z = \pm L_z/2$, where an abrupt drop to $\tau_{zx} = 0$ occurs.

If simple shear is to produce an easy-glide fabric in exposed volume V of the specimen, τ_{zx} must dominate σ during creep deformation. A creep test began with elastic deformation producing the linear σ_{xx} and parabolic τ_{zx} distribution along L_z shown in Figure 6. The ratio of exposed specimen lengths L_x and L_z needed for τ_{zx} to dominate σ
$\bar{\sigma}$ is the average absolute value of σ_{xx}, then:

$$\bar{\sigma}L_z = \int_{-L_z/2}^{+L_z/2} \sigma_{xx}\,dz = 2\int_{0}^{L_z/2} \sigma \qquad = \tfrac{1}{2}\sigma \qquad (13)$$

The bending moment M_y about y at the box grips is therefore:

$$M_y = \left[\frac{2}{3}\left(+\frac{L_z}{2}\right)\right]\left[\frac{1}{2}L_zL_y(+\bar{\sigma})\right] + \left[\frac{2}{3}\left(-\frac{L_z}{2}\right)\right]\left[\frac{1}{2}L_zL_y(-\bar{\sigma})\right]$$

$$= \tfrac{1}{3}L_yL_z^2\bar{\sigma} = \tfrac{1}{3}L_yL_z^2\sigma_m \qquad (14)$$

where lever-arms $\pm\frac{1}{3}L_z$ act on forces $\pm\frac{1}{2}L_zL_y\bar{\sigma}$, and $\bar{\sigma} = \frac{1}{2}\sigma_m$.

$$\bar{\tau}L_z = \int_{-L_z/2}^{+L_z/2} \tau_{zx}\,dz = \int_{-L_z/2}^{+L_z/2} \tau_m\left[1 - (2z/L_z)^2\right]dz = \frac{2}{3}\tau_mL_z\,. \qquad (15)$$

The bending moment about y at the box grips is therefore:

$$M_y = \left[L_x\right]\left[L_yL_z\bar{\tau}\right] = L_xL_yL_z\bar{\tau} = \frac{2}{3}L_xL_yL_z\tau_m\,. \qquad (16)$$

Equating Equations (14) and (16) for equilibrium gives:

$$\bar{\sigma} = \tfrac{1}{2}\sigma_m = 2\left(L_x/L_z\right)\tau_m = 3\left(L_x/L_z\right)\bar{\tau}\,. \qquad (17)$$

The creep test was ended when recrystallization produced an easy-glide ice fabric that mimicked plastic deformation (Hughes, 1977, fig. 23). Hence, $\bar{\sigma} = \sigma_m$ except at $z = 0$ and $\bar{\tau} = \tau_m$ except at $z = \pm L_z/2$. Therefore:

$$M_y = \left[\frac{1}{2}\left(+\frac{L_z}{z}\right)\right]\left[\frac{1}{2}L_zL_y(+\bar{\sigma})\right] + \left[\frac{1}{2}\left(-\frac{L_z}{z}\right)\right]\left[\frac{1}{2}L_zL_y(-\bar{\sigma})\right]$$

$$= \frac{1}{4}L_yL_z^2\bar{\sigma} \qquad \frac{1}{4}\,y\,z\,\sigma_m$$

$$= \left[L_x\right]\left[L_yL_z\bar{\tau}\right] = L_xL_yL_z\bar{\tau} = L_xL_yL_z\tau_m \qquad (18)$$

for which

$$\bar{\sigma} = \sigma_m = 4\left(L_x/L_z\right)\bar{\tau} = 4\left(L_x/L_z\right)\tau_m\,. \qquad (19)$$

We conclude from Equations (17) and (19) that τ_{zx} will dominate σ

We conducted creep experiments with $L_x = 10$ mm and $L_x = 20$ mm, both for $L_z = 75$ mm. Recrystallization produced an easy-glide fabric in both cases. Slight bending at the box grips was observed for $L_x = 20$ mm, but none for $L_x = 10$ mm. Bending was monitored by freezing cross-hair threads into the ice specimen in order to compare local shear strain $\epsilon_{zx} = \frac{1}{2}(\partial u_z/\partial x + \partial u_x/z) = \Delta u_z/2\Delta L_x$ midway between the box grips with shear strain $\epsilon_{zx} = \frac{1}{2}\tan\gamma = u_z/2L_x$ between the box grips. Box grips were used to prevent bending from detaching the specimen from the grips where bending stress σ_{xx} was tensile and produced convex bends, as observed by Rigsby (1958).

Our laboratory creep experiments were conducted at −3°C, the mean annual temperature on Deception Island, and recrystallization invariably occurred when the applied shear stress approached 1 bar (100 kPa) and shear strain approached 10%. To illustrate this, Figure 7 compares creep data at −3°C for $\tau_{zx} = 55$ kPa and $\tau_{zx} = 117$ kPa. At 55 kPa, recrystallization had not begun after 4 months, the time between the 12 August 1970 volcanic eruption that produced the ice wall on Deception Island and our initial observations of shear bands in the ice wall. In Figure 7, 1100 h of creep at 55 kPa had produced $\epsilon_{zx} = 0.05$ and a steady-state strain-rate of $\dot{\epsilon}_{zx} = 0.40$/a. At 117 kPa,

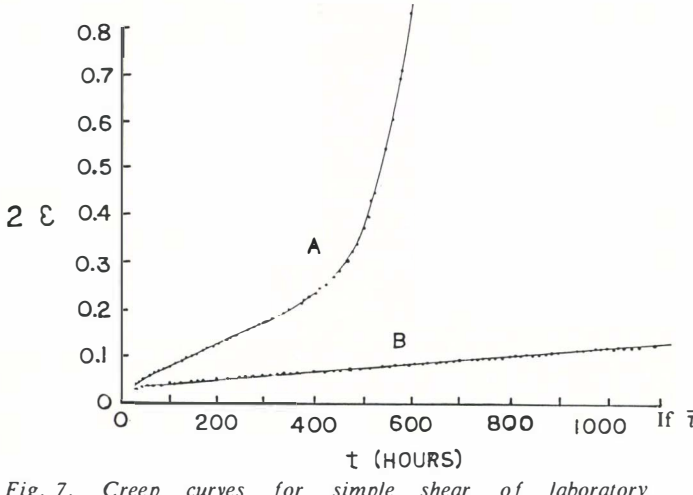

Fig. 7. Creep curves for simple shear of laboratory polycrystalline ice conducted at −3°C using the creep configuration in Figure 5 to duplicate the shear bands in the calving ice wall on Deception Island. Curve A: $\tau_{zx} = 117$ kPa; curve B: $\tau_{zx} = 55$ kPa.

recrystallization began at $\varepsilon_{zx} = 0.08$ after 300 h of creep and ended at $\varepsilon_{zx} = 0.40$ after 300 additional hours of creep, to produce a steady-state strain-rate of $\dot{\varepsilon}_{zx} = 1.9/a$ before recrystallization and $\dot{\varepsilon}_{zx} = 24/a$ after recrystallization.

Measurements of the size and fabric of grains after recrystallization showed that ice in deformed volume V had an average grain diameter of 5 mm, compared to 1 mm before recrystallization, and that recrystallization had converted the random grain fabric into a single-maximum fabric in which optic axes were clustered tighly about a pole lying 90° from the plane of shear. Figures 8 and 9 show the grain-size and fabric after recrystallization. Even

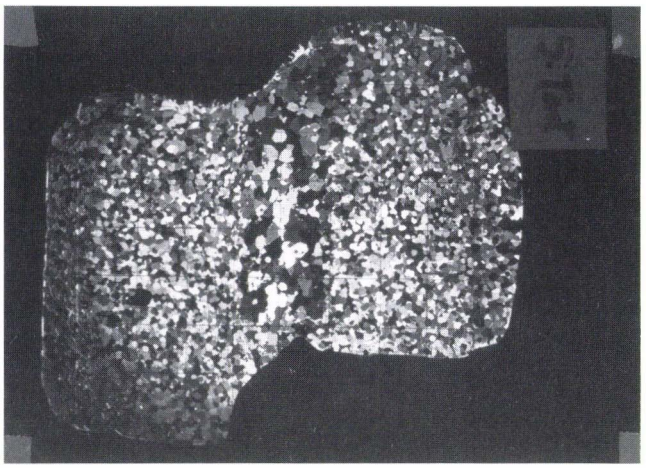

Fig. 8. Grain-sizes in a thin section made from the ice specimen sheared in a laboratory creep experiment to produce the data for curve A in Figure 7. Recrystallization in the plane of shear was accompanied by grain growth.

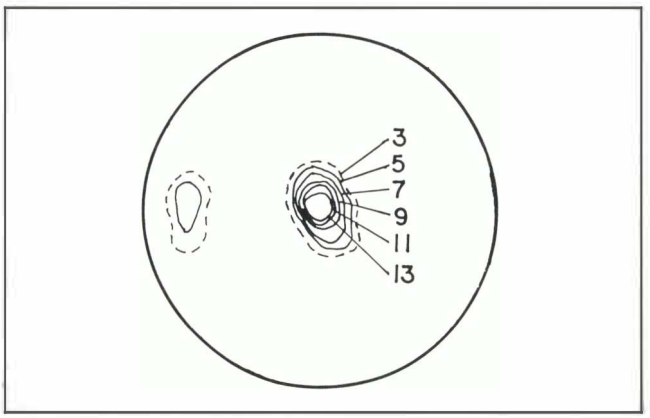

Fig. 9. The ice fabric in the recrystallized part of the thin section in Figure 8. A single-maximum fabric exists in the plane of shear. Numbers denote the per cent of c-axes per 1% of area in the Schmidt diagram for 165 poles inside the shear band.

with a 5 mm diameter, sheared length L_z of the specimen includes about 15 grains, so the increase in grain-size should not invalidate the creep experiments. Interestingly, the 5 mm diameter of recrystallized grains was also the most common grain-size in the Deception Island ice wall, both in and between shear bands. As is seen by comparing Figures 4 and 9, the single-maximum fabric for easy glide was much stronger in our laboratory creep experiments than in the Deception Island shear bands, even though total strain was much greater in the Deception Island shear bands. This may be because the original fabric was random in our laboratory ice but had a single-maximum fabric at 45° to the shear bands in Deception Island ice, a fabric that was retained between shear bands and even survived recrystallization in the shear bands, where it was weakened but not detroyed.

Recrystallization in the laboratory ice increased the strain-rate over ten-fold, from $\dot{\gamma} = 4.3 \times 10^{-4}/h$ to $\dot{\gamma} = 5.5 \times 10^{-3}/h$; that is, from $\dot{\varepsilon}_{zx} = 1.88/a$ to $\dot{\varepsilon}_{zx} = 24.1/a$. We believe a drastic strain-rate increase of this order leads to shear rupture and slab calving along the ice wall on Deception Island, an increase that takes place in only about 300 h when the shear stress is about 1 bar. This is the shear stress for slab calving that is predicted by Equations (8) through (10) for ice walls when crevasses open about 10 m behind the wall, a common occurrence, and by Equation (11) for under-water block calving.

Our creep data allow a calculation of viscoplastic exponent n and hardness parameter A in the flow of ice for our close approximation to simple shear:

$$\dot{\varepsilon}_{zx} = (\tau_{zx}/A)^n. \tag{20}$$

Using the creep data in Figure 7 as an example, if the two minimum strain-rates and applied shear stresses before recrystallization are designated by subscripts 1 and 2, respectively, Equation (20) gives $n = \ln[(\dot{\varepsilon}_{zx})_1/(\dot{\varepsilon}_{zx})_2]/\ln[(\tau_{zx})_1/(\tau_{zx})_2] = 2.07$. This value of n is then used to obtain $A = 86.3\ \text{kPa a}^{1/n}$ and $A = 25.2\ \text{kPa a}^{1/n}$ before and after recrystallization, respectively, from Equation (20) and the two sets of $\dot{\varepsilon}_{zx}$ and τ_{zx} data in Figure 7.

Our creep experiments gave $n \cong 2$, which can be interpreted in two ways. First, following Weertman (1983), perhaps $n \cong 1$ for $\tau_{zx} < 10$ kPa, $n \cong 3$ for 10 kPa $< \tau_{zx} <$ 100 kPa, and $n > 3$ for $\tau_{zx} > 100$ kPa. On this basis, we should expect $n \cong 3$ in our experiments. Secondly, following Hughes (1981), perhaps $n \cong 1$ for transient creep and $n \cong 3$ for steady-state creep. In this case, $n \cong 2$ implies that recrystallization began during transient creep in our creep experiment at 117 kPa, so that in Figure 7 the minimum creep rate at 117 kPa was not the true steady-state creep rate, whereas the minimum creep rate at 55 kPa was the true steady-state creep rate because recrystallization did not occur. Favoring this interpretation is the observation from polar ice sheets and ice shelves that $n \cong 1$ when transient creep is important (Doake and Wolff, 1985; Weertman, 1985), and a component of transient creep would exist in our ice specimens because the distribution of τ_{zx} across L_z changes from parabolic to nearly constant during the creep test even though the applied τ_{zx} was constant. Opposing this interpretation are the creep data by Duval (1976), who found that $n \cong 3$ for both transient and steady-state creep (Hughes, 1985). Although both field and laboratory studies give $n \cong 3$ as the most common value (Paterson, 1981), lower values have been reported. Colbeck and Evans (1973) obtained $n = 1.3$ for Blue Glacier, for example.

Our creep experiments gave unusually low values of hardness parameter A, both before and after recrystallization. Most published creep data report a softness parameter B, which is obtained from the flow law $\dot{\varepsilon}_{zx} = B\tau_{zx}^n$ in our creep experiments, so that $B = A^{-n}$ from Equation (20). Converting A into B from our data for $n = 2.07$ gives $B = 3.15 \times 10^{-12}\ \text{kPa}^{-n}\ \text{s}^{-1}$ before recrystallization and $B = 4.02 \times 10^{-11}\ \text{kPa}^{-n}\ \text{s}^{-1}$ after recrystallization. Equivalent values for $n = 3$ would be $B = 3.74 \times 10^{-14}\ \text{kPa}^{-n}\ \text{s}^{-1}$ before recrystallization and $B = 4.77 \times 10^{-13}\ \text{kPa}^{-n}\ \text{s}^{-1}$ after recrystallization. Paterson (1981, table 3.1) presented field data from temperate glaciers ranging from $n = 2.8$ and $B = 8.85 \times 10^{-15}\ \text{kPa}^{-n}\ \text{a}^{-1}$ to $n = 5.2$ and $B = 5.06 \times 10^{-20}\ \text{kPa}^{-n}\ \text{a}^{-1}$. Paterson (1981, table 3.2) presented laboratory data for the minimum creep rate in our stress range at or near −2°C. These data give a mean value of $B = 2.7 \times 10^{-15}\ \text{kPa}^{-n}\ \text{s}^{-1}$ standardized for $n = 3$, but the largest value was ten times the smallest value. Our values of B standardized for $n = 3$ are outside the upper end of that range by a factor of 2.8 before recrystallization and by a factor of 35 after recrystallization. We conclude that our value of B is close to the usual range for minimum creep rates before recrystallization, but is unique after recrystallization.

The differences between our laboratory creep data and those tabulated by Paterson (1981) may be explained by the different states of stress. The Paterson (1981) data were for creep in uniaxial compression, in which the compressive stress was uniform across the specimen cross-section. Our data were for creep in simple shear, in which the shear stress varied across the specimen cross-section from zero at the sides to a maximum at the center, and only became relatively uniform after recrystallization. Consequently,

recrystallization was not uniform; it began in the center and spread to the sides.

CONCLUSIONS

Calving ice walls are found grounded on dry land, along beaches, and in water. We have concluded that (1) in all these environments the rate-controlling calving mechanism is bending creep that produces nearly vertical shear bands in the ice wall, and leads to shear rupture along these bands, (2) the calving rate is accurately predicted by a calving formula based on this mechanism, using data from a calving ice wall on Deception Island, and (3) calving follows shear rupture at a shear stress of about 1 bar.

These results are fortunate because they (1) extend the calving formula developed for the Deception Island ice wall to all calving ice walls in all environments, (2) spare us from addressing turbulent flow, the one great unsolved problem of classical physics because, without bending creep, wave action would control the calving rate in beach and aquatic environments, and (3) allow us to incorporate the calving rate along with the melting rate in computer models that simulate advance and retreat of continental ice sheets in polar, lacustrine, and marine environments, where ice walls are grounded on land, along beaches, or in water.

ACKNOWLEDGEMENTS

Our field and laboratory studies of the Deception Island calving ice wall were conducted during 1970–74, H. Brecher, R. Curl, C. Parkinson, and M. Scholz assisting in the field work. The calving mechanism and its universal application to ice walls emerged when one of us (T.H.) had opportunities to revisit the Deception Island ice wall and other ice walls along the Antarctic Peninsula and in the Chilean fjords during the 1982–83 and 1988–89 austral summers, through the courtesy of Salén Lindblad Cruises and Society Expeditions Cruises. This work was supported by U.S. National Science Foundation grants GV-36510 and DPP-8312196, and by Battelle, P.N.L., subcontract B-R7112-A-E.

REFERENCES

Colbeck, S.C. and R.J. Evans. 1973. A flow law for temperate glacier ice. *J. Glaciol.*, **12**(64), 71-86.

Dehlinger, U. 1950. The experimental and theoretical results of plasticity at normal speeds of strain. *In Symposium on Plastic Deformation of Crystalline Solids*. Pittsburgh, Mellon Institute, 103-110.

Doake, C.S.M. and E.W. Wolff. 1985. Flow law for ice in polar ice sheets. *Nature*, 314(6008), 255-257.

Duval, P. 1976. Lois du fluage transitoire ou permanent de la glace polycristalline pour divers états de contrainte. *Ann. Geophys.*, 32(4), 335-350.

Garofalo, F., O. Richmond, and W.F. Domis. 1962. Design of apparatus for constant-stress or constant-load creep tests. *J. Basic Eng.*, **84**, 287-293.

Hughes, T. 1971. Nonhomogeneous strain studies on Antarctic glaciers. *Antarct. J. U.S.*, **6**(4), 89-90.

Hughes, T. 1977. West Antarctic ice streams. *Rev. Geophys. Space Phys.*, 15(1), 1-46.

Hughes, T. 1981. Lithosphere deformation by continental ice sheets. *Proc. R. Soc. London, Ser. A*, 378(1775), 507-527.

Hughes, T. 1985. Thermal convection in ice sheets: we look but do not see. *J. Glaciol.*, 31(107), 39-48.

Hughes, T. 1989. Calving ice walls. *Ann. Glaciol.*, **12**, 74-80.

Paterson, W.S.B. 1981. *The physics of glaciers. Second edition*. Oxford, etc., Pergamon Press.

Post, A. and R. LaChapelle. 1971. *Glacier ice*. Seattle, University of Washington Press.

Read, W.T. 1950. Discussion following paper by U. Dehlinger, 1950: The experimental and theoretical results of plasticity at normal speeds of strain. *In Symposium on Plastic Deformation of Crystalline Solids*, Pittsburgh, Mellon Institute, 111-112.

Rigsby, G.P. 1958. Effect of hydrostatic pressure on velocity of shear deformation of single ice crystals. *J. Glaciol.*, 3(24), 273-278.

Weertman, J. 1983. Creep deformation of ice. *Annu. Rev. Earth Planet. Sci.*, **11**, 215-240.

Weertman, J. 1985. Unsolved problems of creep. *Nature*, 314(6008), 227.

MS. received 19 September 1988 and in revised form 22 March 1989